World Journal of Chemical Education, 2022, Vol. 10, No. 2, 76-83
Available online at http://pubs.sciepub.com/wjce/10/2/4
Published by Science and Education Publishing
DOI:10.12691/wjce-10-2-4

Study of Magnetic Interactions in Dy^{3+} Substituted $Zn_{0.5}Mg_{0.5}Dy_xFe_{2-x}O_4$ Ferrites

Sahi Ram*, Shailndra Singh

Mössbauer Laboratory, Department of Physics, Jai Narain Vyas University, Jodhpur, Rajasthan, India - 342001
*Corresponding author: sr_panwar@yahoo.co.in

Received April 05, 2022; Revised May 09, 2022; Accepted May 19, 2022

Abstract Rare earth dysprosium substituted spinel ferrites with a composition of $Zn_{0.5}Mg_{0.5}Dy_xFe_{2-x}O_4$ (x = 0.0, 0.02, 0.10 and 0.20) were synthesized by the solid-state reaction method. X-ray diffraction studies revealed the formation of single-phase cubic structures for all compositions. The lattice constant and crystallite size varied with increasing Dy^{3+} content in the Zn-Mg ferrite. ^{57}Fe Mössbauer spectroscopic studies were carried out to determine the chemical state of iron, its occupancy and relative amount in tetrahedral (A) sites, octahedral (B) sites or both. The obtained value of relative amount of iron in the tetrahedral (A) site, octahedral (B) site or both was used to obtain the cation distribution at the tetrahedral (A) and octahedral (B) sites. The cation distribution was used to determine the cation-cation distances, cation-anion distances and inter-ionic bond angles to understand the spin interactions and the impact of Dy^{3+} ion substitution on magnetic interactions in substituted Zn-Mg ferrites.

Keywords: *spinel ferrite, cation distribution, Mössbauer spectroscopy, magnetic materials*

Cite This Article: Sahi Ram, and Shailndra Singh, "Study of Magnetic Interactions in Dy^{3+} Substituted $Zn_{0.5}Mg_{0.5}Dy_xFe_{2-x}O_4$ Ferrites." *World Journal of Chemical Education*, vol. 10, no. 2 (2022): 76-83. doi: 10.12691/wjce-10-2-4.

1. Introduction

Ferrites are ferrimagnetic materials that exhibit spontaneous magnetization at room temperature and magnetic properties that are identical to those of ferromagnetic materials. Along with their good magnetic properties, ferrites have high electrical resistivity, low dielectric and low eddy current losses [1]. Nano structured ferrites are becoming versatile assets owing to their excellent magnetic properties compared to those of bulk-sized ferrites [2].

Zn-Mg ferrite is a mixed spinel ferrite synthesized by substituting Zn into $MgFe_2O_4$. The $MgFe_2O_4$ is an inverse spinel ferrite that exhibit ferromagnetic nature. In $MgFe_2O_4$ the magnetic properties are attributed to only Fe^{3+} ions because the divalent Mg^{2+} ion is diamagnetic in nature (μ_B= 0). The distribution of Fe^{3+} in tetrahedral site constitute magnetic sublattice-A and distribution of Fe^{3+} in octahedral site constitutes magnetic sublattice-B. The net magnetization is due to the difference in magnetic moments of sublattice-B and sublattice-A. The substitution of Zn^{2+} ions in to $MgFe_2O_4$ makes a mixed spinel Zn-Mg ferrite. The Zn^{2+} ion has a preferred occupancy of tetrahedral (A) site [3] and occupy tetrahedral (A) site while Mg^{2+} ion can occupy both sites.

Many workers [4-8] have studied the $Zn_xMg_{1-x}Fe_2O_4$ composition (for $0 \leq x \leq 1.0$) and reported the changes in structural and magnetic properties with increase in Zn content. All reported Zn-Mg ferrite compositions exhibit ferromagnetic behavior. $Zn_{0.5}Mg_{0.5}Fe_2O_4$ has been reported to have maximum magnetization value. $Zn_{0.5}Mg_{0.5}Fe_2O_4$ ferrite is a soft magnetic material and net magnetization contribution is due to the combined magnetic moments of magnetic sublattice-A and sublattice-B. Because the divalent ions Zn^{2+} and Mg^{2+} are diamagnetic in nature and have zero contribution to the net magnetic moment, the magnetization of sublattice-A and sublattice-B in Zn-Mg ferrite will be due to the presence of Fe^{3+} magnetic ions. It is clear that in Zn-Mg ferrites, the magnetization of sublattice-A and sublattice-B will also change if there is a variation in the occupancy of Fe^{3+} ions in the tetrahedral and octahedral sites.

Several workers [9,10,11] have reported that when Fe^{3+} ions in ferrite are substituted by rare-earth ions, there is a substantial change in the structural and magnetic properties. The magnetic properties are improved owing to the increase in the magneto crystalline anisotropy, coercivity and saturation magnetization [12,13]. The isotropic or anisotropic nature of the coercivity and saturation magnetization is in accordance to the variation in the contribution of the f-electron orbital to magnetic interaction [14]. The magnetic properties of ferrites are influenced by the anti ferromagnetic super exchange interaction between adjoining Fe^{3+} ions. When rare earth ions substitutes Fe^{3+} ions in spinel ferrite, RE^{3+}-Fe^{3+} interaction is induced, which modifies the intrinsic magnetic properties. In ferrites, because of larger distance between the cations, the exchange interactions are favoured by oxygen anions and are termed super exchange interactions. The super exchange interaction also plays a

crucial role in the buildup of intrinsic magnetism in spinel structures. The interactions between cations via oxygen anions can be A-B and A-A or B-B interactions. In A-B interaction, all magnetic spins at the A-site are aligned in one direction and constitute magnetic sublattice-A while all magnetic spins at the B-site align in a direction opposite to the direction of the spins at the A-site and form magnetic sublattice-B, resulting in net magnetization in ferrite. The net magnetization is given by the difference in the magnetic moments of sublattice-B and sublattice-A. The super-exchange interactions in ferrites are also affected by the distances and angles between the ion pairs in spinel structure. Lakhani V. K. et. al. [15] and Kumar G. et. al, [16] reported that the magnetic interaction in substituted spinel ferrites is much more effective for certain angles and distances between the cation-cation and cation-anion ions. They showed that the distances and angles between ion pairs play a decisive role in spin interaction for certain favorable angles, and that the magnetic interaction is much more effective.

In present study, a series of Dy^{3+} substituted $Zn_{0.5}Mg_{0.5}Dy_xFe_{2-x}O_4$ (x=0.0, 0.02, 0.10 and 0.20) ferrites were synthesized and investigated by X-ray diffraction studies of their structural properties and ^{57}Fe Mössbauer spectroscopic studies to obtain the cation distribution in tetrahedral and octahedral sites and to estimate the magnetic interactions in Dy^{3+} substituted $Zn_{0.5}Mg_{0.5}Fe_2O_4$ ferrites.

2. Experimental

The rare earth Dy^{3+} ions substituted Zn-Mg ferrite with compositions $Zn_{0.5}Mg_{0.5}Dy_xFe_{2-x}O_4$ (x=0.0, 0.02, 0.10 and 0.20) were synthesized by solid state reaction method. Analytic grade metal oxides (purity 99.9%) ZnO, MgO, Dy_2O and Fe_2O_3 were weighed in stochiometric proportion and mixed thoroughly in a liquid medium. The mixture is then calcinated at 600°C to obtain fine homogeneous sample. The calcinated mixture is finally sintered at 1180°C for 11 hours. The sintered material was kept for cooling down at room temperature before using it for characterizations. The scanning electron micrographs were taken to confirm the homogeneity of the samples. For X-ray studies, the PANalytical X'pert Pro MPD diffractometer using Cu-Kα radiation was used to collect the x-ray diffraction patterns at 2^0 per minute scanning rate from 10^0 to 80^0 range of 2θ. The indexing and refinement of all peaks was done using "FullProf programme [17].

Mössbauer spectra were recorded at room temperature (300K) with a conventional constant acceleration spectrometer using a 10 mCi ^{57}CO source embedded in Rhodium matrix. Details of the experimental set-up are similar as reported earlier by Nigam *et. al*. [18]. All spectra showing superposition of quadrupole doublets were computer fitted to resolve them using a least square routine computer program written by Meerwall [19] by assuming each spectrum to be sum of Lorentzians functions. During the curve fitting, the width and intensity of the two halves of a quadrupole doublet were constrained to be equal. The quality of the fit was judged from the value of χ^2 which was obtained close to 1.0 per degree of freedom in most of the cases. However, a deviation in the value of χ^2 has been accepted in some occasion when iterations did not improve the value of χ^2. The isomer shift (IS) value is reported with respect to the spectrum of standard iron foil of 25 μm thickness. Solid lines in the spectra reported here represent computer fitted curve and dots represent the experimental points.

3. Results and Discussion

The x-ray diffraction patterns obtained for Dy^{3+} ions substituted Zn-Mg ferrite with compositions $Zn_{0.5}Mg_{0.5}Dy_xFe_{2-x}O_4$ (x=0.0, 0.02, 0.10 and 0.20) are displayed in Figure 1. The peaks indexed as (220), (311), (400), (422), (511) and (440) matches with (JCPDS card number 00-008-0234) to confirm the formation of single phase cubic spinel structure in all samples. In sample with $x \leq 0.02$, the presence of single phase cubic structure indicates the partial incorporation of Dy^{3+} ions into spinel structure. In sample with $x > 0.02$ some additional peaks corresponding to secondary phase $DyFeO_3$ are also present along with regular peaks of spinel structure [20]. For higher concentration of Dy^{3+} ions, the presence of secondary phase at grain boundary is expected because the larger ionic radii Dy^{3+} ions has preferential occupancy to the octahedral site [21]. This secondary phase tends to induce lattice distortion either due to the compression caused by discrepancy in thermal expansion coefficient between bulk and inter-granular material or due to the mismatch in grain and boundary phases. The lattice constant 'a' was calculated by using the relation $a = d\sqrt{h^2 + k^2 + l^2}$, where (hkl) is the index of the XRD reflection peak and 'd' is the inter-planar spacing. The crystallite size 'D' of the samples was calculated as per the Debye-Scherrer equation [22].

$$D = \frac{0.9\lambda}{\beta cos\theta}$$

Where λ is x-ray wavelength of Cu-Kα radiation (1.54 Å), β is the full width at half maximum of (311) peak and θ is diffraction angle. The x-ray parameters obtained in present study are listed in Table 1.

Table 1. X-ray parameters obtained in $Zn_{0.5}Mg_{0.5}Dy_xFe_{2-x}O_4$ (x = 0, 0.02, 0.10 and 0.20) ferrites

Dy Content (x)	Lattice Parameter (Å)	Crystallite Size (nm)	X-Ray Density ρ_x (g/cm^3)	Lattice Strain η (×10^{-2})
0.0	8.4123	53.2	4.920	1.048
0.02	8.4151	52	4.963	1.073
0.10	8.4216	51.5	5.141	1.083
0.20	8.4232	51	5.375	1.093

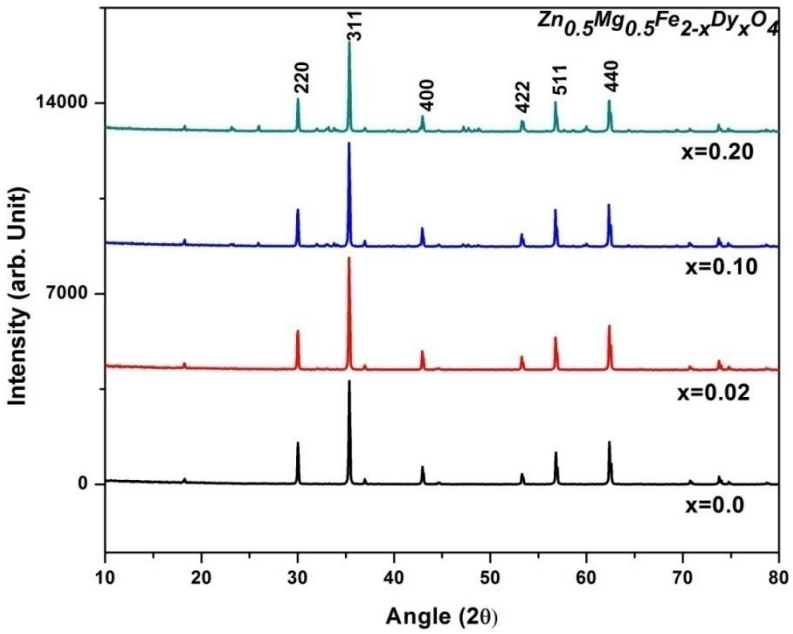

Figure 1. X-ray diffraction patterns obtained in $Zn_{0.5}Mg_{0.5}Dy_xFe_{2-x}O_4$ (x = 0.0, 0.02, 0.10 and 0.20) ferrites

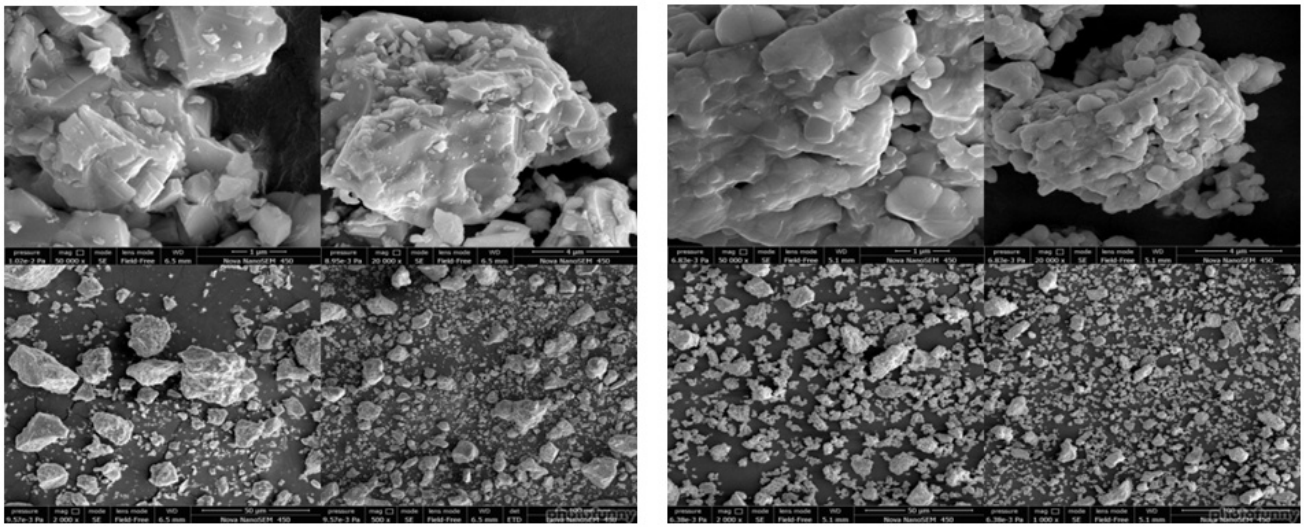

Figure 2. SEM micrograph of (a) $Zn_{0.5}Mg_{0.5}Fe_2O_4$; (b) $Zn_{0.5}Mg_{0.5}Dy_{0.20}Fe_{1.80}O_4$

The average crystallite size was observed in the range 53.2 nm to 51 nm. This decrease in crystallite size with increasing concentration of Dy substitution is expected because larger ionic radii Dy^{3+} ion (0.91 Å) preferentially occupies the octahedral site and may reside partially at the grain boundary and cause pressure on the grain resulting to obstruction of the growth of crystal [23].

Typical scanning electron micrographs displayed in Figure 2 indicate well packed compact arrangement of homogenous and agglomerated particles forming uneven sized crystallite like grains. The agglomeration of particles is visible in all compositions. In case of pure composition (x=0), the agglomeration of particles is due to the magnetic interaction among the particles [24]. In Dy substituted compositions, the agglomeration is due to magnetic interaction between particles as well as also due to the accumulation of some Dy^{3+} ions at grain boundary without replacing Fe^{3+} ions in octahedral site [25]. This type of agglomeration results in restriction of crystal growth and hence reduction in crystallite size with increasing Dy content as obtained in XRD studies.

The Mössbauer spectra of all synthesized samples recorded at room temperature are displayed in Figure 3. The concentration of Dy^{3+} substitutions is mentioned in the figure itself. The Mössbauer parameters obtained by the least square fitting of Lorentzians lines are given in Table 2. The isomer shift (IS) value is reported with respect to the spectrum of standard iron foil of 25μm thickness. In present study, the Isomer shift values are obtained ranging from 0.1 mm/s to 0.4 mm/s which attributes to iron in Fe^{3+} state [26,27]. The assignment of iron in Fe^{3+}state occupying either tetrahedral site or octahedral site is done in accordance with earlier reported work [28,29]. The doublet with higher value of isomer shift is assigned to iron in Fe^{3+} state occupying the tetrahedral site (A) while the doublet with smaller value of isomer shift is assigned to iron in Fe^{3+} state occupying the octahedral site (B).

Table 2. Mossbauer parameters obtained in $Zn_{0.5}Mg_{0.5}Dy_xFe_{2-x}O_4$ (x = 0, 0.02, 0.10 and 0.20) Ferrites

Dy Content (x)	Doublet		IS mms^{-1}	QS mms^{-1}	LW	RA
0.0	I	Fe^{3+} A-Site	0.38	0.20	0.44	24.63
	II	Fe^{3+} B-Site	0.13	0.32	0.30	75.37
0.02	I	Fe^{3+} A-Site	0.39	0.80	0.34	10.6
	II	Fe^{3+} B-Site	0.14	0.28	0.24	89.4
0.10	I	Fe^{3+} B-Site	0.14	0.30	0.32	100.0
0.20	I	Fe^{3+} A-Site	0.22	0.41	0.37	13.0
	II	Fe^{3+} B-Site	0.14	0.15	0.51	87.0

From Table 2, it can be seen that in pure sample (x=0.0) the isomer shift value for site A is greater than that of site B. In a similar study on Zn-Mg ferrites, Wang J. et. Al. [28] has also reported this trend of larger isomer shift value of site-A in comparison to that of site-B. The samples with Dy concentration x=0.10 exhibits only one central doublet which is attributed to the magnetically isolated Fe^{3+} ion and does not show magnetic ordering due to surrounding non magnetic particles [30].

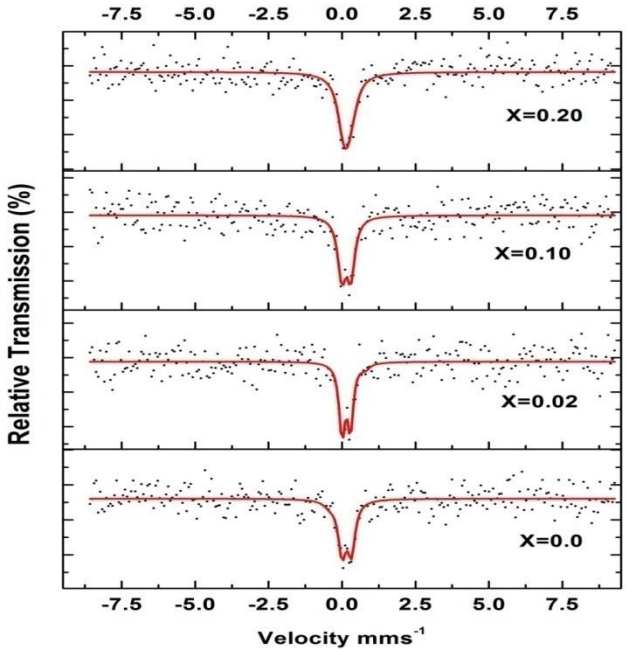

Figure 3. Room temperature Mössbauer spectra of $Zn_{0.5}Mg_{0.5}Dy_xFe_{2-x}O_4$ (x = 0, 0.02, 0.10 and 0.20) ferrites

The amount of iron in Fe^{3+} state occupying the tetrahedral site (A) iron in Fe^{3+} state occupying octahedral site (B) can be estimated by the relative area of the two quadruple doublets [31]. In pure sample (x=0.0), the distribution of Fe^{3+} ions into A-site and B-site clearly indicate the formation of inverse spinel structure. This formation of inverse spinel Zn-Mg ferrite (x=0) is obvious due to the tendency of divalent ions Zn^{2+} having preferential occupancy to A-site while Mg^{2+} having preferential occupancy to B-site [32,33].

From Table 2, it can also be seen that for increasing concentration of Dy substitution, the relative amount of iron in tetrahedral site reduces while in octahedral site it increases. This clearly reflects the migration of Fe^{3+} ions towards octahedral site. It is obvious that the Fe^{3+} ions migrated from tetrahedral site to octahedral site will replace the Mg^{2+} ions from octahedral site because Dy^{3+} ions due to their larger ionic radii (0.91 Å) has preferential occupancy only to octahedral site.

In composition with x = 0.10, the Mössbauer spectrum exhibit only one central doublet corresponding to Fe^{3+} ion only in B-site. It reflects the complete migration of Fe^{3+} from tetrahedral site to octahedral site by replacing Mg^{2+} so that the tetrahedral site now has only divalent ions Zn^{2+} and Mg^{2+} while the octahedral site has only trivalent ions Fe^{3+} and Dy^{3+}. As earlier reported by Suwalka et. al. [31], the cation distribution of tetrahedral site and octahedral site in all compositions is estimated from Mössbauer spectra and is given in Table 3.

Table 3. Estimated cation distribution in $Zn_{0.5}Mg_{0.5}Dy_xFe_{2-x}O_4$ (x = 0, 0.02, 0.10 and 0.20) ferrites

Dy Content (x)	A-site	B-site
0.0	$(Zn^{2+}_{0.5}\ Mg^{2+}_{0.007}\ Fe^{3+}_{0.493})$	$[Mg^{2+}_{0.493}\ Fe^{3+}_{1.507}]$
0.02	$(Zn^{2+}_{0.5}\ Mg^{2+}_{0.290}\ Fe^{3+}_{0.210})$	$[Mg^{2+}_{0.210}\ Dy^{3+}_{0.02}\ Fe^{3+}_{1.770}]$
0.10	$(Zn^{2+}_{0.5}\ Mg^{2+}_{0.5})$	$[Dy^{3+}_{0.10}\ Fe^{3+}_{1.90}]$
0.20	$(Zn^{2+}_{0.5}\ Mg^{2+}_{0.266}\ Fe^{3+}_{0.234})$	$[Mg^{2+}_{0.234}\ Dy^{3+}_{0.20}\ Fe^{3+}_{1.566}]$

Using the cation distribution given in Table 3, the average ionic radii at the tetrahedral site (r_A) and at octahedral sites (r_B) in all samples can be calculated by following relations [34]

$$r_A = \left[\begin{array}{l}\left(C^A_{Zn^{2+}}\right)\left(r_{Zn^{2+}}\right)+\left(C^A_{Mg^{2+}}\right)\left(r_{Mg^{2+}}\right)\\ +\left(C^A_{Dy^{3+}}\right)\left(r_{Dy^{3+}}\right)+\left(C^A_{Fe^{3+}}\right)\left(r_{Fe^{3+}}\right)\end{array}\right] \quad (1)$$

$$r_B = \frac{1}{2}\left[\begin{array}{l}\left(C^B_{Zn^{2+}}\right)\left(r_{Zn^{2+}}\right)+\left(C^B_{Mg^{2+}}\right)\left(r_{Mg^{2+}}\right)\\ +\left(C^B_{Dy^{3+}}\right)\left(r_{Dy^{3+}}\right)+\left(C^B_{Fe^{3+}}\right)\left(r_{Fe^{3+}}\right)\end{array}\right] \quad (2)$$

Where C^A and C^B are the ionic concentration in A-site and B-sites respectively, $r_{Zn^{2+}}$, $r_{Mg^{2+}}$, $r_{Dy^{3+}}$, and $r_{Fe^{3+}}$, are the radii of Zn^{2+}, Mg^{2+}, Dy^{3+} and Fe^{3+} respectively.

Table 4. Lattice constant (a_{exp}), mean ionic radius of tetrahedral site (r_A) and octahedral site (r_B), theoretical value of Lattice constant (a_{th}) and oxygen positional parameter (u) in $Zn_{0.5}Mg_{0.5}Dy_xFe_{2-x}O_4$ (x = 0, 0.02, 0.10 and 0.20) ferrites

Dy Content (x)	a_{exp} (Å)	r_A (Å)	r_B (Å)	a_{th} (Å)	u^{3m} (1/4, 1/4, 1/4)	u^{43m} (3/8, 3/8, 3/8)		
0.0	8.4123	0.705	0.667	8.4163	0.2642	0.3892	0.3889	0.3891
0.02	8.4151	0.702	0.671	8.4224	0.2639	0.3889	0.3886	0.3888
0.10	8.4216	0.700	0.682	8.4486	0.2633	0.3883	0.3880	0.3883
0.20	8.4232	0.702	0.692	8.4784	0.2629	0.3879	0.3877	0.3879

Using the values of radii of tetrahedral A-site (r_A) and mean radii of octahedral B-site (r_B), the theoretical values of lattice constant a_{th} for all samples can be obtained by the relation [35]

$$a_{th} = \frac{8}{3\sqrt{3}}\left[(r_A + R_o) + \sqrt{3}(r_B + R_o)\right] \quad (3)$$

here R_0 is the radius of oxygen ion (R_0 = 1.32 Å).

The calculated values of mean ionic radii of tetrahedral A-site (r_A), mean ionic radii of octahedral B-site (r_B) and calculated value of lattice constant 'a_{th}' are listed in Table 4.

It is seen from Table 4 that in the sample (x=0) the mean ionic radii of tetrahedral site is more that the mean ionic radii of octahedral site. It is obvious because the tetrahedral site is occupied by Zn^{2+} having ionic radius (0.74 Å) larger than the ionic radius of Mg^{2+} ions (0.66 Å) which occupy octahedral site. When Dy^{3+} ions are substituted with increasing concentration, the mean ionic radii of octahedral site increases but mean ionic radii of tetrahedral site show subtle change and remain almost unchanged. The increase in mean ionic radii is obviously due to the large ionic radii (0.91 Å) of Dy^{3+} ions [36,37]. The Dy^{3+} ions have preferred occupancy to octahedral site because of larger interstices space in octahedral site. The Dy^{3+} ion replaces Fe^{3+} ions in octahedral site, moreover from cation distribution given in Table 3, it is clear that the Fe^{3+} ions replaces Mg^{2+} ions from octahedral site and cause the migration of Mg^{2+} ions to tetrahedral site. The ions involved in the compositions are having different ionic radii can cause a distortion in crystal symmetry. The distortion is also due to the internal stress by large ionic radii Dy^{3+} ions entering in to the octahedral site. The large variation in theoretical value of lattice constant 'a_{th}' in comparison to the experimentally calculated value 'a_{exp}' is attributed to this distortion in crystal symmetry.

Furthermore, as the involved ions have different ionic radii, therefore to accommodate the incumbent ions in to either tetrahedral site or octahedral site, the oxygen anion may suffer a shifting from their actual position. So in spinel structure, the oxygen anion may or may not be present at their exact location in the FCC structure. The variation in position of oxygen anions is described in term of oxygen positional parameter 'u'.

The oxygen positional parameter u^{3m} value for center of symmetry at $(1/4, 1/4, 1/4)$ considering the origin at B-site is calculated by the relation [38]

$$u^{3m} = \frac{\frac{1}{4}R^2 - \frac{2}{3} + \left(\frac{11}{48}R^2 - \frac{1}{18}\right)^{1/2}}{2R^2 - 2} \quad (4)$$

Where $R = \frac{(B-O)}{(A-O)}$, the average bond length $(B-O) = (r_B + R_O)$ and $(A-O) = (r_A + R_O)$ are calculated using the mean ionic radii of A-site (r_A) and mean ionic radii of B-site (r_B) obtained from cation distribution. The R_O corresponds to the ionic radii of oxygen anion (1.32 Å)

The oxygen positional parameter u^{43m} value for center of symmetry at $(3/8, 3/8, 3/8)$ considering the origin at A-site is calculated by the relation [34]

$$u^{43m} = \frac{\frac{1}{2}R^2 - \frac{11}{12} + \left(\frac{11}{48}R^2 - \frac{1}{18}\right)^{1/2}}{2R^2 - 2} \quad (5)$$

$$u^{43m} = \frac{r_A + R_o}{a\sqrt{3}} + \frac{1}{4} \quad (6)$$

$$u^{43m} = 0.3876\left(\frac{r_B}{r_A}\right)^{-0.07054} \quad (7)$$

From Table 4, it can be seen that the three values of u^{43m} of each individual composition are almost same inspite of being calculated by different formulas. For a FCC structure, the ideal value of u^{3m} for origin at B-site is $u^{3m}_{ideal} = 0.250$ Å and the ideal value of u^{43m} for origin at A-site is $u^{43m}_{ideal} = 0.375$ Å.

Generally the ferrites show a deviation from this ideal value of oxygen positional parameter 'u' and attain a larger value of 'u' in comparison to the ideal value [39,40]. The deviation in 'u' value is also obtained in present study. From Table 4, it can be observed that when Dy is substituted into Zn-Mg ferrite, the oxygen positional parameter value is slightly larger in value. However, for further increase in Dy content, the value of 'u' further decreases. The decrease in value of 'u' indicates that the anions at B-site are moving away from cations at octahedral interstices due to the expansion of the octahedral interstices. The displacement of oxygen ions is in such a way that in A-B interaction the distances between A and O ions are unchanged while the distance between B and O ions increases. Using the value of oxygen positional parameter 'u' and experimental value of lattice constant 'a' for each composition, the bond lengths on tetrahedral site (d_{AX}), the bond length on octahedral site (d_{BX}), the length of tetrahedral shared edge (d_{AXE}), the length of octahedral shared edge (d_{BX}) and the unshared octahedral edge length (d_{BXEU}) are calculated by putting in the relations [41]

$$d_{AX} = a\sqrt{3}\left(u^{43m} - \frac{1}{4}\right) \quad (7)$$

$$d_{BX} = a\sqrt{\left[3\left(u^{43m}\right)^2 - \frac{11}{4}u^{43m} + \frac{43}{64}\right]} \quad (8)$$

$$d_{AXE} = a\sqrt{2}\left(2u^{43m} - \frac{1}{2}\right) \quad (9)$$

$$d_{BXE} = a\sqrt{2}\left(1-2u^{43m}\right) \quad (10)$$

$$d_{BXEU} = a\sqrt{\left[4\left(u^{43m}\right)^2 - 3u^{43m} + \frac{11}{16}\right]} \quad (11)$$

The calculated values of bond lengths, shared edge lengths and unshared octahedral edge length are listed in Table 5. The variations of d_{AX} and d_{BX} with increasing Dy content is displayed in Figure 4(a) and the variation of d_{AXE}, d_{BXE}, and d_{BXEU} with increasing content of Dy are displayed in Figure 4(b).

Table 5. Bond lengths at tetrahedral site (d_{AX}), bond length at octahedral site (d_{BX}), shared tetrahedral edge length (d_{AXE}), shared octahedral edge length (d_{BXE}) and unshared octahedral edge (d_{BXEU}) in $Zn_{0.5}Mg_{0.5}Dy_xFe_{2-x}O_4$ (x = 0, 0.02, 0.10 and 0.20) ferrites

Dy Content (x)	d_{AX} (Å)	d_{BX} (Å)	d_{AXE} (Å)	d_{BXE} (Å)	d_{BXEU} (Å)
0.0	2.0292	1.9917	3.3136	2.6376	2.9852
0.02	2.0263	1.9954	3.3089	2.6466	2.9869
0.10	2.0238	2.0061	3.3048	2.6692	2.9955
0.20	2.0251	2.0162	3.3069	2.6882	3.0055

With the substitution of Dy^{3+} ion content, the bond length and edge length on tetrahedral site does not change but the bond length and edge length on octahedral site increases. The unshared edge length on octahedral site also remain unchanged but slightly increases at higher concentration of Dy^{3+} ions substitution (x=0.10 and 0.20). This observed trend of bond lengths and edge lengths is in conformity with the observed ionic radii of tetrahedral site and octahedral site indicating the expansion in octahedral site.

The inter-ionic distances the cation-cation (M_e-M_e) (b, c, d, e, and f) and between cation-anion (M_e-O) (p, q, r and s) has been calculated using the experimental value of lattice constant (a_{exp}) and oxygen positional parameter (u^{3m}) in the following relations [41]

$$M_e - M_e$$

$$b = \left(\frac{a}{4}\right)\sqrt{2}$$

$$c = \left(\frac{a}{8}\right)\sqrt{11}$$

$$d = \left(\frac{a}{4}\right)\sqrt{3}$$

$$e = \left(\frac{3a}{8}\right)\sqrt{3}$$

$$f = \left(\frac{a}{4}\right)\sqrt{6}$$

$$M_e - O$$

$$p = a\left(\frac{1}{2} - u^{3m}\right)$$

$$q = a\left(u^{3m} - \frac{1}{8}\right)\sqrt{3}$$

$$r = a\left(u^{3m} - \frac{1}{8}\right)\sqrt{11}$$

$$s = \frac{a}{3}\left(u^{3m} + \frac{1}{2}\right)\sqrt{3}$$

Using the values of inter-ionic distance between cation-cation and cation-anion, the bond angles are calculated by following relations [15]

$$\theta_1 = \cos^{-1}\left[\frac{p^2+q^2-c^2}{2pq}\right]$$

$$\theta_2 = \cos^{-1}\left[\frac{p^2+r^2-e^2}{2pr}\right]$$

$$\theta_3 = \cos^{-1}\left[\frac{2p^2-b^2}{2p^2}\right]$$

$$\theta_4 = \cos^{-1}\left[\frac{p^2+s^2-f^2}{2ps}\right]$$

$$\theta_5 = \cos^{-1}\left[\frac{r^2+q^2-d^2}{2rq}\right]$$

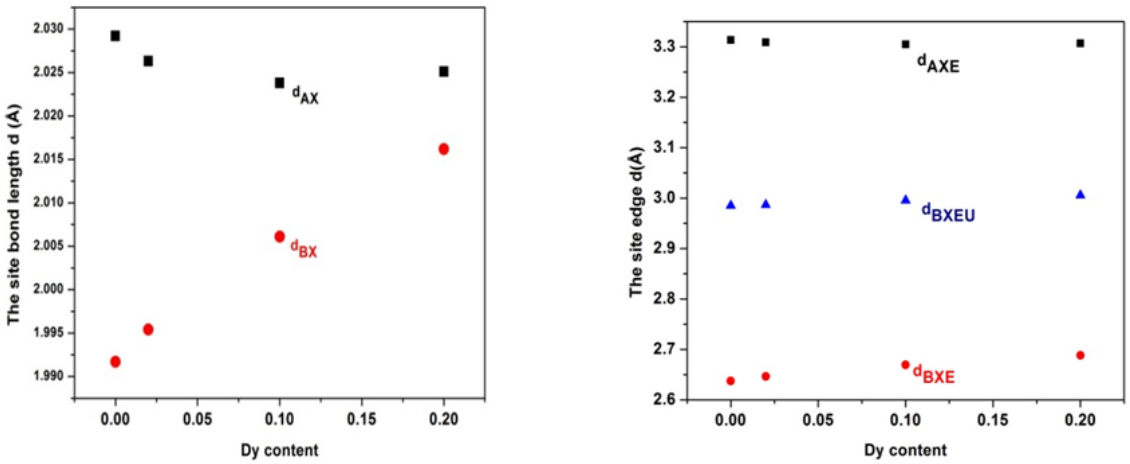

Figure 4. Variations of (a) site bond length and (b) site edge with Dy^{3+} content

The calculated values of inter-ionic distances between cation-cation, cation-anion and bond angles are listed in Table 6. It is noted that with increasing Dy content the inter-ionic distance between cation-cation and cation-anion distance also increases slowly (except q and r). Since the inter-ionic distances are related to the lattice constant, the small increase in inter-ionic distance with Dy content (x) is in agreement with small increase in lattice constant 'a_{exp}'. In composition with larger Dy content (x=0.20), the bond length and shared edge length of tetrahedral site is slightly increases. This distinct pattern is attributed to large sized Dy^{3+} ions accumulated at the boundary and cause partial stretching of tetrahedral site away from octahedral site.

Table 6. Cation-cation distances (b, c, d, e, f), cation-anion distances (p, q, r, s) and inter-ionic bond angles obtained in $Zn_{0.5}Mg_{0.5}Dy_xFe_{2-x}O_4$ (x = 0, 0.02, 0.10 and 0.20) ferrites

Cation-Cation distances $(M_e - M_e)$	Dy Content (x)			
	0.0	0.02	0.10	0.20
b (Å)	2.9742	2.9752	2.9775	2.9781
c (Å)	3.4875	3.4887	3.4914	3.4921
d (Å)	3.6426	3.6438	3.6466	3.6473
e (Å)	5.4639	5.4658	5.4699	5.4710
f (Å)	5.1514	5.1532	5.1571	5.1581
Cation-Anion distances $(M_e - O)$				
p (Å)	1.9836	1.9868	1.9934	1.9971
q (Å)	2.0282	2.0245	2.0173	2.0119
r (Å)	3.8837	3.8766	3.8629	3.8525
s (Å)	3.7116	3.7114	3.7113	3.7101
Inter-ionic angles (degree)				
θ_1	120.757	120.852	121.041	121.168
θ_2	134.698	135.042	135.715	136.18
θ_3	97.1312	96.9659	96.6375	96.4252
θ_4	126.832	126.801	126.731	126.687
θ_5	67.8973	68.1225	68.574	68.8777

The bond angles θ_1, θ_2 and θ_5 corresponds to super exchange A-B and A-A interaction while the bond angle θ_3 and θ_4 corresponds to B-B interactions. The strength of interactions is directly proportional to the bond angle and inversely proportional to the bond length. With increase in Dy^{3+} ion content, the angles θ_1, θ_2 and θ_5 increases and the angles θ_3 and θ_4 decrease. This increase in angles θ_1, θ_2 and θ_5 correspond to the strengthening of super exchange A-B interactions. The decrease in angles θ_3 and θ_4 indicates the weakening in B-B interaction. However, from Table 5 and Figure 4, it is noted that with increasing Dy^{3+} content the bond length and shared edge length at octahedral site increases. This increase in bond length weakens the A-B interaction despite the increase in bond angles.

4. Conclusion

The substitution of Dy^{3+} ions in Zn-Mg ferrite done by solid state reaction method resulted into the synthesis of $Zn_{0.5}Mg_{0.5}Dy_xFe_{2-x}O_4$ (x = 0, 0.02, 0.10 and 0.20) ferrites. With the substitution of larger ionic radii Dy^{3+} ion in to B-site of Zn-Mg ferrite, the structural properties are found to change with increase in Dy content. The substitution of Dy^{3+} ions in Zn-Mg ferrite has also changed the cation distribution of tetrahedral site and octahedral site. The cation distribution changes drastically with increase in Dy content. Furthermore, with the inclusion of Dy^{3+} ion in increasing concentration, the variation of bond angles indicates the strengthening of super exchange interaction but the increase in bond length of octahedral site and the increasing trend of cation-cation inter-ionic distances contradicts. It is inferred that in Dy^{3+} substituted Zn-Mg ferrites, magnetic properties are expected to improve. In compositions with large concentration of Dy substitution, a hindrance to magnetic properties is also expected. The magnetic interactions in Dy-substituted Zn-Mg ferrite indicate change in microscopic magnetic properties

Acknowledgements

Authors are thankful to Department of Physics, Jai Narain Vyas University Jodhpur for providing the research facilities to carry out x-ray diffraction study and Mössbauer Spectroscopic study. One of the authors Shailndra Singh is thankful to University Grants Commission (UGC), New Delhi for providing the UGC-BSR doctoral fellowship.

Declaration

The manuscript has been prepared through contributions of all authors. All authors have given approval to the final version of the manuscript. All authors declare that they have no conflicts of interest.

References

[1] Hashim, M.; Alimuddin; Kumar, S.; Ali, S.; Koo, B. H.; Chung, H.; Kumar, R., "Structural, magnetic and electrical properties of Al^{3+} substituted Ni–Zn ferrite nanoparticles J. Alloys Compd., Vol. 511(1), pp. 107-114 (2012).

[2] Ott, G., Wrba J. and Lucke, R., "Recent developments of Mn–Zn ferrites for high permeability applications" J. Magn. Magn. Mater., Vol. 254-255, pp. 535-537 (2003).

[3] Thummer, K. P., Chhantbar, M. C., Modi, K. B., Baldha, G. J. and Joshi, H. H., "Localized canted spin behavior in $Zn_xMg_{1.5-x}Mn_{0.5}FeO_4$ spinel ferrite system" J. Magn. Magn. Mater., Vol. 280(1), pp. 23-30 (2004).

[4] Manikandan, A., Judith Vijaya, J., Sundararajan, M., Meghanathan, C., John Kennedy, L. and Bououdina, M., "Optical and magnetic properties of Mg-doped $ZnFe_2O_4$ nanoparticles prepared by rapid microwave combustion method", SuperLatt. And Microstr., Vol. 64, pp.118-131 (2013).

[5] Rodriguez-Reyes, P. Y., Hernandez-Cortes, D. A., Escobedo-Bocardo, J. C., Almanza-Robles, J. M., Sanchez-Fuentes, H. J., Jasso-Teran, A., De-Leon-Prado, L. E., Mendez-Nonell, J. and HurTado-Lopez, G. F., " Structural and magnetic properties of Mg-Zn ferrites ($Mg_{1-x}Zn_xFe_2O_4$) prepared by sol-gel method", J. Magn. Magn. Mater., Vol. 427, pp. 268-271 (2017).

[6] Choodamani, C., Rudraswamy, B. and Chandrappa, G.T., "Structural, electrical, and magnetic properties of zn substituted magnesium ferrite", Ceram. Int., Vol. 42(9), pp. 10565-10571 (2016).

[7] Goya, G. F. and Rechenberg, H. R., "Ionic disorder and Néel temperature in $ZnFe_2O_4$ nanoparticles" J. Magn. Magn. Mater., Vol. 196-197, pp. 191-192 (1999).

[8] Masina, P., Moyo, T. and Abdallah, H. M. I., "Synthesis, structural and magnetic properties of $Zn_xMg_{1-x}Fe_2O_4$ nanoferrites", J. Magn. Magn. Mater., Vol. 381, pp. 41-49 (2015).

[9] Phor, L., and Kumar, V., "Structural, magnetic and dielectric properties of lanthanum substituted $Mn_{0.5}Zn_{0.5}Fe_2O_4$", Ceram. Int., Vol. 45, pp. 22972-22980 (2019).

[10] Pachpinde, A.M., Langade, M.M., Lohar, K. S., Patange, S.M. and Sagar, E. S, "Impact of larger rare earth Pr^{3+} ions on the physical properties of chemically derived $Pr_xCoFe_{2-x}O_4$ nanoparticles", Chemical physics", Vol. 429, pp. 20-26 (2014)

[11] Rezlescu, N., Rezlescu, E., Pasnicu, C. and Craus, M. L., "Effects of the rare-earth ions on some properties of a nickel-zinc ferrite", J. Phys: Condens Matter., Vol. 6, pp. 5707-5716 (1994).

[12] Biao, Z., Ya-Wen, Z., Chun-Sheng, L/, Chun-Hua, Y., Liang-Yao, C. and Song-You, W., "Rare-earth-mediated magnetism and magneto-optical Kerr effects in nanocrystalline $CoFeMn_{0.9}RE_{0.1}O_4$ thin films", J. Magn. Magn. Mater., Vol. 280(2-3), pp. 327-333 (2004).

[13] Peng, J., Hojamberdiev, M., Xu, Y., Cao, B., Wang, J. and Wu, H., "Hydrothermal synthesis and magnetic properties of gadolinium-doped $CoFe_2O_4$ nanoparticles", J. Magn. Magn. Mater., Vol. 323(1), pp. 133-137 (2011).

[14] Akamatsu, H., Kawabata, J., Fujita, K., Murai, S. and Tanaka, K., "Magnetic properties of oxide glasses containing iron and rare earth ions", Phys. Rev. B 84, 144408 (2011).

[15] Lakhani, V. K., Pathak, T. K., Vasoya, N. H. and Modi, K. B., " Structural parameters snd x-ray Debye temperature determination study on copper-ferrite-aluminates", Solid State Sci., Vol. 13, pp. 539-547 (2011).

[16] Kumar, G., Singh, V. P., Kumar, A., Shah, J., Kumar, S., Chauhan, B. S., Kotnala, R. K. and Singh, M., "Estimation of magnetic interactions in substituted Mg-Mn ferrites synthesized via citrate precursor technique", Adv. Mater. Lett., Vol. 6(9), pp. 828-833 (2015).

[17] Rodriguez-Carvajal, B, "Recent developments of the program FULLPROF, commission on powder diffraction", IUCr. Newsl., Vol. 26 (2001).

[18] Nigam, A.N., Tripathi, R.P., Singh, H.S., Gambhir, R.S. and Lukose, N.G., "Mössbauer studies on Ghotaru Well No.1 of Jaisalmer Basin", Fuel, Vol. 68(2), pp. 209-212 (1989).

[19] Meerwall, E. V., "A least-square spectral curve fitting routine for strongly overlapping Lorentzians or Gaussians", Computer physics communications, Vol. 9, pp.117-128 (1975).

[20] Zipare, K. V., Bandgar, S. S. and Shahane, G. S., "Effect of Dy-substitution on structural and magnetic properties of Mn-Zn ferrite nanoparticles", J. Rare Earths, Vol. 36, pp. 86-94 (2018).

[21] Ahmed, M. A., Ateia, E. and El-Dek, S. I., "Rare earth doping effect on the structural and electrical properties of Mg–Ti ferrite", Mat. Lett., Vol. 57 (26-27), pp. 4255-4266 (2003).

[22] Cullity, B. D. and Stock, S. R., "Elements of X-ray diffraction", Third Ed. Prentice-Hall, New York", (2001).

[23] Mohseni, H., Shokrollahi, H., Sharifi, I. and Gheisari, K., "Magnetic and structural studies of the Mn-doped Mg–Zn ferrite nanoparticles synthesized by the glycine nitrate process", J. Magn. Magn. Mater., Vol. 324, no. 22, pp 3741-3747 (2012).

[24] Rahman, S., Nadeem, K., Anis-ur-Rehman, M., Mumtaz, M., Naeem, S. and Letofsky-Papst, I., "Structural and magnetic properties of ZnMg-ferrite nanoparticles prepared using the co-precipitation method", Ceram. Int., Vol. 39, pp. 5235-5239 (2013).

[25] Anwar, A., Zulfiqar, S., Yousuf, M. A., Ragab, S. A., Khan, M. A., Shakir, I. and Warsi, M. F., "Impact of rare earth Dy^{3+} cations on the various parameters of nanocrystalline nickel spinel ferrite" J. Mater. Res. Technol., Vol. 9(3), pp. 5313-5325 (2020)

[26] Kumar, S., Farea, A.M.M., Batoo, K.M., Lee, C.G., Koo, B.H. and Yonsef, A., "Mössbauer studies of $Co_{0.5}Cd_xFe_{2.5-x}O_4$ ($0.0 \leq x \leq 0.5$) ferrite", Physica B: Condensed matter, Vol. 403 (19-20), pp. 3604-3607 (2008).

[27] Eltabey, M.M., Massoud, A.M. and Radu, C., "Microstructure and Superparamagnetic Properties of Mg-Ni-Cd Ferrites Nanoparticles", Journal of nanomaterials, Vol. 204, pp. 492832 (2014).

[28] Wang, J., Zeng, C., Peng, Z. and Chen, Q., "Synthesis and magnetic properties of $Zn_{1-x}Mn_xFe_2O_4$ nanoparticles" Physica B" Vol. 349 (1-4), pp. 124-128 (2004).

[29] Sreeja, V., Vijyanand, S., Deka, S. and Joy, P., "Magnetic and Mössbauer spectroscopic studies of NiZn ferrite nanoparticles synthesized by a combustion method". Hyperfine interaction, Vol. 183(1-3), pp. 99-107 (2008).

[30] Gupta, M. and Randhawa, B.S., "Mössbauer, magnetic and electric studies on mixed Rb–Zn ferrites prepared by solution combustion method", Mat. Chem. and phys., Vol. 130, pp. 513-518 (2011).

[31] Suwalka, O., Sharma, R. K., Sebastian, V., Laxm,i N. and Venogopalan, K., "A study of nanosized Ni substituted Co-Zn ferrite prepared by coprecipitation", J. Magn. Magn. Mater., Vol. 313, 198-203 (2007).

[32] Mohammed, K.A., Al-Rawas, A.D., Gismelseed, A.M., Setlai, A., Widatallah, H.M., Yousif, A., Elzain, M.E. and Shongwe, M., "Infrared and structural studies of $Mg_{1-x}Zn_xFe_2O_4$ ferrites", Physica B, Vol. 407, pp. 795-804 (2012).

[33] Phor, L., Chahal, S. and Kumar, V., "Zn^{2+} substituted superparamagnetic $MgFe_2O_4$ spinel-ferrites: Investigation on structural and spin-interactions", J. Adv. Ceram., Vol. 9(5), pp. 576-587 (2020).

[34] Globus, A., Pascard, H. and Cagan, V., "Distance between magnetic ions and fundamental properties in ferrite" Journal of Phys. Colloques, Vol. 38, pp. 163-168 (1977).

[35] Mazen, S.A., Abdallah, M.H., Sabrah, B.A., and Hashem, H. A. M., "The Effect of Titanium on Some Physical Properties of $CuFe_2O_4$" Physica Status solidi (a), Vol. 134(1), pp. 263-271 (1992).

[36] Chouhan, B. S., Kumar, R., Jadhav, K. M. and Singh, M., "Magnetic study of substituted Mg-Mn ferrites synthesized by citrate precursor method" J. Magn. Magn. Mater., Vol. 283, p 71 (2005).

[37] Kumar, G., Kanthwal, M., Chauhan, B. S. and Singh, M., " Cation distribution in mixed Mg-Mn ferrites from X-Ray diffraction technique and saturation magnetization", Ind. J. Pure & Appl. Phys., Vol. 44(12), pp. 930-934 (2006).

[38] Zaki, H. M., Al-Heniti, S. H., Elmosalami, T. A., "Structural. magnetic and dielectric studies of copper substituted nano-crystalline spinel magnesium zinc ferrite", J. of Alloys and comp., Vol. 633, pp.104-114 (2015).

[39] Sharma, R. K., Sebastian, V., Lakshmi, N., Venugopalan, K., Raghavendra, R. and Gupta, A., "Variation of structural and hyperfine parameters in nanoparticles of Cr-substituted Co-Zn ferrites", Phys. Rev. B 75, 144419 (2007).

[40] Jani, K. H., Chhantbar, M. and Joshi, H., "Study of magnetic ordering in $MnAl_xCr_xFe_{2-2x}O_4$", J. Magn. Magn. Mater., Vol. 18, pp. 2208-2214 (2008).

[41] Shirsath, S. E., Kadam, R. H., Patange, S. M., Mane, M. L., Ghasemi, A. and Morisako, A., "Enhanced magnetic properties of Dy^{3+} substituted Ni-Cu-Zn ferrite nanoparticles", Appl. Phys. Lett., Vol. 100, 042407 (2012).